This is a repository copy of *Leaf anatomy explains the strength of C4 activity within the grass species Alloteropsis semialata*.

White Rose Research Online URL for this paper:
https://eprints.whiterose.ac.uk/199403/

Version: Published Version

ORIGINAL ARTICLE

Leaf anatomy explains the strength of C$_4$ activity within the grass species *Alloteropsis semialata*

Ahmed S. Alenazi[1,2] | Matheus E. Bianconi[1] | Ella Middlemiss[1] |
Vanja Milenkovic[1] | Emma V. Curran[1] | Graciela Sotelo[1] | Marjorie R. Lundgren[1] |
Florence Nyirenda[3] | Lara Pereira[1] | Pascal-Antoine Christin[1] |
Luke T. Dunning[1] | Colin P. Osborne[4]

[1]Ecology and Evolutionary Biology, School of Biosciences, University of Sheffield, Sheffield, UK

[2]Department of Biological Sciences, Northern Border University, Arar, Saudi Arabia

[3]Department of Biological Sciences, University of Zambia, Lusaka, Zambia

[4]Plants, Photosynthesis and Soil, School of Biosciences, University of Sheffield, Sheffield, UK

Correspondence
Colin P. Osborne, Plants, Photosynthesis and Soil, School of Biosciences, University of Sheffield, Sheffield S10 2TN, UK.
Email: c.p.osborne@sheffield.ac.uk

Abstract

C$_4$ photosynthesis results from anatomical and biochemical characteristics that together concentrate CO$_2$ around ribulose-1,5-bisphosphate carboxylase/oxygenase (Rubisco), increasing productivity in warm conditions. This complex trait evolved through the gradual accumulation of components, and particular species possess only some of these, resulting in weak C$_4$ activity. The consequences of adding C$_4$ components have been modelled and investigated through comparative approaches, but the intraspecific dynamics responsible for strengthening the C$_4$ pathway remain largely unexplored. Here, we evaluate the link between anatomical variation and C$_4$ activity, focusing on populations of the photosynthetically diverse grass *Alloteropsis semialata* that fix various proportions of carbon via the C$_4$ cycle. The carbon isotope ratios in these populations range from values typical of C$_3$ to those typical of C$_4$ plants. This variation is statistically explained by a combination of leaf anatomical traits linked to the preponderance of bundle sheath tissue. We hypothesize that increased investment in bundle sheath boosts the strength of the intercellular C$_4$ pump and shifts the balance of carbon acquisition towards the C$_4$ cycle. Carbon isotope ratios indicating a stronger C$_4$ pathway are associated with warmer, drier environments, suggesting that incremental anatomical alterations can lead to the emergence of C$_4$ physiology during local adaptation within metapopulations.

KEYWORDS
C$_3$–C$_4$ intermediate, C$_4$ photosynthesis, evolution, population genetics

1 | INTRODUCTION

The majority of plants use the ancestral C$_3$ photosynthetic pathway, in which atmospheric CO$_2$ is fixed directly by the enzyme ribulose-1,5-bisphosphate carboxylase/oxygenase (Rubisco) in a reaction that constitutes the entry point of the Calvin–Benson–Bassham cycle. However, Rubisco can also bind O$_2$, which starts the energetically costly photorespiratory pathway (Bowes et al., 1971; Lorimer & Andrews, 1973). The efficiency of the C$_3$ type, therefore, decreases in all conditions that increase the partial pressure of O$_2$ relative to

CO_2 within the leaf (Ku et al., 1983; Peixoto et al., 2021; Sage et al., 2014). These conditions include warm, arid and saline habitats in the low-CO_2 atmosphere that prevailed over the last 30 million years (Sage, 2001, 2004). Plants have evolved a number of strategies to minimize photorespiration costs, the most significant of which are CO_2-concentrating mechanisms, such as C_4 photosynthesis (Edwards & Ku, 1987; Hatch, 1971). In C_4 plants, the initial fixation of carbon is mediated by phosphoenolpyruvate carboxylase (PEPC), an enzyme without affinity for O_2 (Burnell & Hatch, 1988; Hatch & Slack, 1966). This initial reaction usually takes place in the mesophyll of C_4 plants, which CO_2 reaches via simple diffusion through the stomata. The resulting C_4 acid is then transported into a different leaf compartment, usually the bundle sheath that surrounds the veins, where Rubisco is segregated in C_4 plants (Hatch, 1971, 1987). CO_2 is released within this compartment isolated from the atmosphere, and the intermediate compounds of the cycle are brought back to the location of PEPC activity and regenerated (Hatch, 1987). Through this mechanism, the C_4 cycle increases the relative partial pressure of CO_2 around Rubisco, almost completely suppressing photorespiration (von Caemmerer & Furbank, 2003).

The C_4 pathway relies on many anatomical and biochemical novelties compared to the C_3 ancestral state (Hatch, 1987). A number of enzymes, including PEPC and those needed to transform and transport the C_4 acid, release CO_2 and regenerate the intermediate compounds, need to be active at high levels in specific leaf compartments (Hatch, 1971; Hatch & Osmond, 1976). In addition, specific leaf properties are needed to support the segregation of reactions and allow for a rapid transfer of metabolites (Dengler et al., 1994; Hattersley, 1984; Lundgren et al., 2014). In particular, mesophyll and bundle sheath cells need to be in close proximity, with no more than one cell separating them in C_4 plants (Hattersley & Watson, 1975). In addition, a large fraction of the leaf must be dedicated to the tissue that houses the Calvin–Benson–Bassham cycle (Brown & Hattersley, 1989; Dengler & Nelson, 1999). Despite this apparent complexity, the C_4 pathway evolved more than 60 times independently from C_3 ancestors (Sage et al., 2011). This remarkable evolutionary phenomenon is explained by the existence of intermediate stages, which bridge the gap between the C_3 and C_4 states (Edwards & Ku, 1987; Heckmann et al., 2013; Kennedy & Laetsch, 1974; Monson et al., 1984; Sayre & Kennedy, 1977; Williams et al., 2013; Yorimitsu et al., 2019). In particular, some plants fix part of their atmospheric carbon via the C_3 cycle and part via the C_4 cycle, in proportions that vary from weak to strong C_4 involvements (Edwards & Ku, 1987; Monson et al., 1986; Stata et al., 2019). Theoretical models predict the existence of a path from C_3 to C_4, where each step increases photosynthetic efficiency (Heckmann et al., 2013; Monson & Moore, 1989; Williams et al., 2013). However, empirical tests of this hypothesis are largely missing and the detailed events allowing the transition from a weak to a strong C_4 pathway remain unexplored.

Investigating photosynthetic systems and how they respond to environmental gradients can be done effectively using the stable carbon isotope ratio ($\delta^{13}C$; Farquhar et al., 1989; O'Leary, 1981). Plants contain lower levels of ^{13}C than ambient air, and the ^{13}C content of plant tissue largely depends on the photosynthetic pathway (Bender, 1968; Troughton, 1979), although additional variation can be observed in relation to environmental conditions (Guy et al., 1980; Winter, 1981). Rubisco discriminates against ^{13}C and preferentially fixes ^{12}C during photosynthesis (O'Leary, 1981). In contrast, PEPC discriminates less than Rubisco, making the isotopic composition of plant dry matter a useful tool to identify different photosynthetic types (O'Leary, 1981). $\delta^{13}C$ has been widely used as a proxy for photosynthetic type (Bender, 1968; Brown, 1977; von Caemmerer, 1992; Cerling, 1999; Cerros-Tlatilpa & Columbus, 2009; Gowik et al., 2011; Lundgren et al., 2015; Olofsson et al., 2021; Smith & Brown, 1973; Smith & Epstein, 1971; Stata et al., 2019), with values of −10‰ to −15‰ for C_4 species, and −22‰ to −31‰ for C_3 species (95% confidence intervals from the data compilation of Cerling et al., 1997).

Alloteropsis semialata is the only species known to have both C_3 and C_4 genotypes (Ellis, 1974). In addition, some non-C_4 populations of *A. semialata*, found in the grassy ground layer of the Central Zambezian miombo woodlands, perform a weak C_4 cycle in addition to the direct fixation of CO_2 via the C_3 cycle (Dunning et al., 2017; Lundgren et al., 2016). Comparative analyses have shown that their physiology results from the up-regulation of particular C_4 enzymes (Dunning et al., 2019) and the acquisition of C_4-like anatomical characters (Lundgren et al., 2019) compared to C_3 populations. Importantly, the $\delta^{13}C$ of these plants range from values typical of a weak or null C_4 involvement to values indicative of a C_4 cycle responsible for more than half of carbon acquisition (i.e., −15‰ to −22‰; von Caemmerer, 1992, 2000; Lundgren et al., 2015; Monson et al., 1988; Olofsson et al., 2021; Stata & Sage, 2019). These non-C_4 populations of *A. semialata*, therefore, constitute an attractive system for investigating the changes responsible for the transition from a weak to a strong C_4 cycle.

In this study, we compare the leaf anatomy of wild populations of non-C_4 *A. semialata* representing a range of carbon isotope values, to quantify the importance of anatomical changes during the transition from weak to strong C_4 cycles. We first use $\delta^{13}C$, which reflects the proportion of inorganic carbon fixed by Rubisco as opposed to PEPC, to estimate the strength of the C_4 cycle in each individual. We further correlate the average $\delta^{13}C$ values of each population with the local climate to test for links between C_4 activity and environmental conditions. We then use genomic data to establish the history of non-C_4 populations spread across the Central Zambezian miombo woodlands, and we quantitatively describe the leaf anatomy of multiple non-C_4 individuals per population. These data are used to assess the variation for functionally important C_4 leaf characters and test for relationships with the strength of the C_4 cycle across the phylogenetic tree for this species. Our work sheds new light on the role of ecological variation in driving leaf anatomical changes responsible for the transition from weak to strong C_4 cycles.

2 | MATERIALS AND METHODS

2.1 | Plant sampling and carbon isotopes

Our sampling focused on the Central Zambezian woodlands, where non-C₄ *A. semialata* are known to occur (Bianconi et al., 2020; Lundgren et al., 2016). Populations were collected irrespective of their photosynthetic type in Tanzania and Zambia between 2014 and 2019 (Olofsson et al., 2021), and all 28 populations that included individuals with a non-C₄ carbon isotope ratio ($\delta^{13}C < -17‰$) were selected for analyses in this study. The carbon isotope threshold was chosen based on previous observations of photosynthetic physiology in comparison with $\delta^{13}C$ in this species (Lundgren et al., 2016) and in other groups (Stata & Sage, 2019). This existing sampling was augmented during a field trip to Zambia in January 2020. All populations of *A. semialata*, localized during random walk-and-search stops, were again collected irrespective of their photosynthetic type. Leaf samples of multiple individuals were placed in silica gel and in 70% ethanol, and Global Positioning System (GPS) coordinates were recorded for each locality (Supporting Information: Table S1). In addition, herbarium collections were used to increase geographical coverage. Four previously analysed herbarium samples (Lundgren et al., 2015; Olofsson et al., 2016) and eight new ones from Burundi and the Democratic Republic of Congo (DRC) were included here (Supporting Information: Table S1). The GPS coordinates were used to retrieve for each locality the values of 18 bioclimatic variables from the WorldClim database (Fick & Hijmans, 2017), using the Raster package (Hijmans, 2021) from R (R Core Team, 2020). These data represent the average climate for the region from 1970 to 2000 (Fick & Hijmans, 2017).

Values of $\delta^{13}C$ were retrieved from previous studies or generated here (Supporting Information: Table S1; Bianconi et al., 2020; Lundgren et al., 2015; Olofsson et al., 2021). For the new samples, 1–2 mg of dried tissue of leaves were used to measure the $\delta^{13}C$ with an ANCAGSL preparation module that is joined to a 20–20 stable isotope analyser (PDZ Europa). The $\delta^{13}C$ was expressed relative to the standard Pee Dee Belemnite, and all samples with a $\delta^{13}C < -17‰$ were considered as non-C₄. When sufficient material was available, the $\delta^{13}C$ of non-C₄ individuals that were selected for anatomical analyses were measured three times independently. The median of these three technical replicates was used in subsequent analyses (Supporting Information: Table S2). For the 16 samples where there was insufficient material to replicate the measurements, the use of an unreplicated value reduces the precision of $\delta^{13}C$ estimates. However, the exclusion of these values from the regression analyses did not qualitatively change the results.

To help interpret the $\delta^{13}C$ estimates, we carried out a sensitivity analysis using simple models of carbon isotope discrimination (von Caemmerer, 1992; Farquhar et al., 1982). The analysis particularly emphasized the effects of variation in water-use efficiency via the ratio of intercellular to atmospheric CO_2 partial pressures ($_{pi}/p_a$), and bundle sheath leakiness (ϕ), in plants with a weak C₄ cycle (i.e. 'type II' C₃–C₄ intermediates; Monson et al., 1986).

2.2 | Genome scan and phylogenetic analyses

The phylogenetic relationships among all individuals were inferred by combining sequence data obtained with different approaches. The reduced representation sequencing approach of Olofsson, Dunning et al. (2019) was used to scan the genomes of samples stored in silica gel. Genomic DNA was extracted with the DNeasy Plant Mini Kit (Qiagen). Two restriction enzymes (*Eco*RI and *Mse*I) were used to digest the extracted DNA, and a barcode and a common adapter were ligated. Standard Illumina primers were then added through PCR, with 16 cycles. Each sample was individually barcoded and pools of up to 96 libraries were size selected (target of 300–600 bp) and sequenced as 125 paired-end reads on an Illumina HiSeq. 2500. The new data were combined with the subset of those from Olofsson et al. (2021) corresponding to non-C₄ individuals. The whole genomes of the new herbarium samples were sequenced as 150 bp paired-end Illumina reads at low coverage, using the approach of Olofsson et al. (2016). Existing whole-genome sequence data for other *Alloteropsis* samples representing the multiple lineages of *A. semialata* as well as the other species in the genus were added to the data set (Supporting Information: Table S3; Bianconi et al., 2020; Lundgren et al., 2015; Olofsson et al., 2016).

A nuclear phylogenetic tree was inferred using the method of Bianconi et al. (2020). For each of the 7408 putative single-copy genes in Panicoideae grasses identified by Bianconi et al. (2020), orthologous sequences of *A. semialata* retrieved from the species chromosome-level genome assembly (reference AUS1; Dunning et al., 2019) were used as a reference to map the paired-end reads from all sequence data sets using Bowtie2 v. 2.3.5 (Langmead & Salzberg, 2012) with default parameters. Using a bash-scripted pipeline that implements the mpileup function of Samtools v.1.9 (Li et al., 2009) for variant calling, gene sequences were reconstructed by incorporating variant sites into a consensus sequence as in Olofsson, Cantera et al. (2019). All polymorphic sites were called as ambiguous bases. This method produces sequences that are already aligned to the reference. Gene alignments were trimmed with TrimAl v.1.4 (Gutiérrez-Rodríguez et al., 2009) to remove sites with missing data in more than 50% of individuals. For each gene alignment, individuals with sequences shorter than 100 bp after trimming were removed. In the end, individuals with more than 95% missing data across gene alignments were discarded. The remaining trimmed gene alignments were concatenated, resulting in a 223 023 bp alignment encompassing 252 samples. A maximum likelihood phylogenetic tree was inferred with RAxML v.8.2.12 (Stamatakis, 2014), using the GTRCAT substitution model and 100 bootstrap pseudoreplicates.

2.3 | Microscopy and leaf anatomical measurements

Leaf material collected in the field was fixed and dehydrated in ethanol before embedding. For a minimum of three randomly sampled individuals per population (or all individuals for populations

where fewer than three non-C_4 individuals were located in the field), leaf fragments of 5–7 mm in length were embedded using the Technovit Kit (Technovit 7100; Heraeus Kulzer GmbH). In all cases, these samples for anatomy were taken from the same plant at the same time as the $\delta^{13}C$ samples. For herbarium samples or individuals only available as silica gel dried material, the leaves were first rehydrated in 1% KOH solution for 24 h in the refrigerator at 4°C. After embedding, 11-µm-thick transverse sections were obtained with a rotary microtome (Leica Biosystems) and were stained with 1% Toluidine Blue O for 1.5 min (Sigma-Aldrich). The slides were photographed using an Olympus BX51 microscope with a mounted camera (Olympus). To recreate large stretches of leaf tissue in a cross-section, sequences of images taken along a single leaf were stitched together using the Hugin software (Hugin Development Team, 2015).

All measurements of leaf anatomical properties were made using ImageJ v.1.53f (Schneider et al., 2012). For each leaf, a segment connecting the vertical mid-axis of two consecutive secondary veins (recognized by the presence of metaxylem) was selected, avoiding the midrib and leaf edges (Supporting Information: Figure S1a). For each segment, the total areas in the cross-section of mesophyll (including airspace), outer bundle sheath, inner bundle sheath, and vascular tissue were measured. The proportion of the photosynthetic part of the leaf dedicated to the refixation of carbon acquired via the C_4 cycle, which is the inner bundle sheath also known as the mestome sheath in *A. semialata* (Hattersley et al., 1977), was calculated relative to the mesophyll as the area of inner sheath divided by the sum of the areas of mesophyll and inner bundle sheath (i.e., inner bundle sheath fraction; IBSF).

The number of veins was recorded separately for tertiary veins, which are associated with extraxylary fibres and epidermis thinning, and lower-order veins, which are smaller than tertiary veins and lack extraxylary fibres (hereafter referred to as 'minor veins'). The segment length was measured along a line connecting the centres of secondary and tertiary veins (referred to as 'major veins') and used to calculate the average interveinal distance based on secondary and tertiary veins. The average minimum distance between the outside of the outer sheath of consecutive bundles (including minor veins) was measured as a proxy for the maximum distance between mesophyll and inner bundle sheath cells (i.e., bundle sheath distance, BSD). The size of individual inner sheath cells was measured as the average width of the most equatorial cells of each tertiary vein within the segment (i.e., inner bundle sheath width, IBSW) (Supporting Information: Figure S1).

2.4 | Statistical analyses

All analyses were done in R version 3.6.3. (R Core Team, 2018). The climatic variation among populations was summarized using a principal component analysis with the *prcomp* function in R (R Core Team, 2018). The first two principal components were extracted and used as explanatory variables in multiple linear models. Multiple regression analyses were first used to test for the effects of these climatic variables on photosynthetic diversity, as inferred from the median of $\delta^{13}C$ per population. Photosynthetic diversity within populations was not considered in this analysis since the climate as measured here does not vary within populations. The least significant variable was successively removed until all remaining variables were significant.

Second, we also used multiple regression analysis to test for relationships between $\delta^{13}C$ and anatomical traits, accounting for lineage as a fixed effect. The least significant variable was successively removed until all remaining variables were significant.

Finally, to take phylogenetic relationships into account, phylogenetic generalized least-squares (PGLS) analysis was also carried out in R using the caper package (Orme et al., 2022) using the phylogenetic tree and anatomical traits as explanatory variables. We ran the model with the least significant variable removed until only significant variables ($p < 0.05$) remained. The phylogeny described relationships among the sampled populations, but did not include the relationships among individuals within each population. To run this analysis, we therefore only included the individual from each population that was used to construct the phylogeny.

3 | RESULTS

3.1 | Plant sampling captures a range of carbon isotope ratios

Across all 842 *A. semialata* individuals analysed previously (Bianconi et al., 2020; Lundgren et al., 2015; Olofsson et al., 2021) or here, the value of $\delta^{13}C$ ranges from −9.1‰ to −29.0‰ (Figure 1 and Supporting Information: Table S1). Within the Central Zambezian region, both C_4 individuals with $\delta^{13}C$ above −17‰ and non-C_4 individuals with $\delta^{13}C$ below −17‰ are found (Figure 1), as previously reported (Lundgren et al., 2015, 2016; Olofsson et al., 2016, 2021). In addition to the five populations previously identified (Olofsson et al., 2021), C_4 and non-C_4 individuals were found in sympatry in three new populations (Figure 1). In total, 38 populations from the Central Zambezian region contained non-C_4 individuals based on $\delta^{13}C$ values, which is consistent with previous reports from this region (Bianconi et al., 2020; Dunning et al., 2017; Lundgren et al., 2016). The $\delta^{13}C$ of the 231 non-C_4 collected from these populations range from −27.2‰ to −18.2‰ (Figure 1b), consistent with variation among individuals in the proportion of carbon fixed by C_4 photosynthesis. In addition to the variation among populations, the $\delta^{13}C$ also varied within populations (Supporting Information: Table S1 and Figure S2).

The $\delta^{13}C$ of the 109 non-C_4 individuals selected for anatomical analyses covered the extreme values from this range (Figure 1b and Supporting Information: Table S5). Of these 109 individuals, 55 had $\delta^{13}C$ above −23‰, which indicates a significant involvement of the C_4 cycle in atmospheric CO_2 capture (Stata & Sage, 2019). The selected samples, therefore, represent a panel of non-C_4 accessions with a diversity of C_4 cycle strength (Figure 1b).
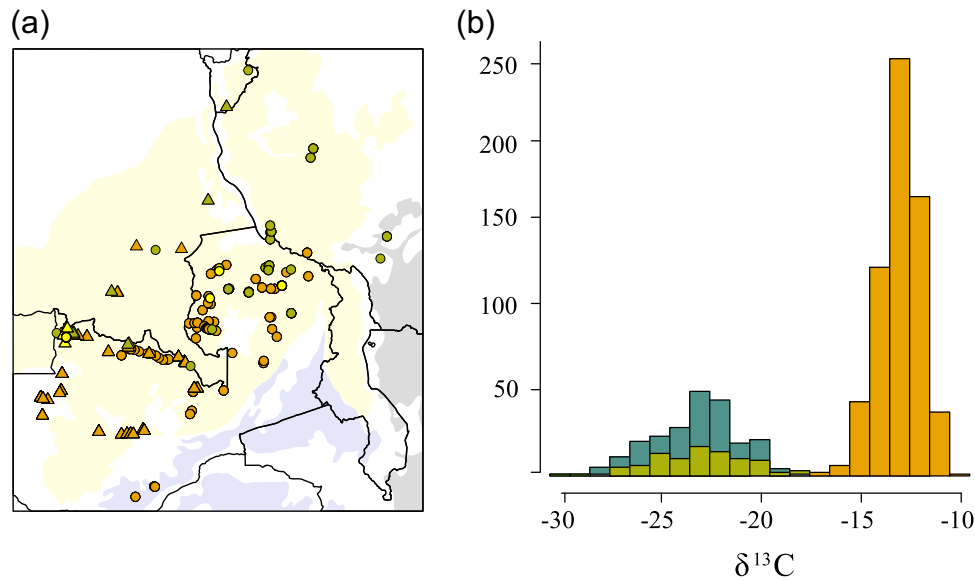
FIGURE 1 Photosynthetic diversity of *Alloteropsis semialata* in Central Zambezian miombo woodlands. (a) Sampled populations are indicated, in orange for those containing only C₄ individuals, in olive green for those containing only non-C₄ individuals, and in yellow for those containing both C₄ and non-C₄ individuals. Previously published populations are shown with circles and newly published ones with triangles. The approximate extent of miombo woodland biogeographic regions is shown in the background, in light yellow for the Central Zambezian woodlands, in light grey for the Eastern Zambezian woodlands and in light blue for Southern Zambezian woodlands (distribution based on Maquia et al., 2019). (b) Distribution of stable carbon isotope ratios for all individuals of *A. semialata* sampled from this region is represented with a histogram (see Supporting Information: Table S1 for details). Values indicative of a C₄ type are in orange, while those indicative of a non-C₄ type are in olive green for individuals sampled for leaf anatomy and in pine green for other non-C₄ individuals. [Color figure can be viewed at wileyonlinelibrary.com]

3.2 │ Ecology affects the strength of the C₄ cycle

The first axis of the principal component analysis on climatic variables explains 63.1% of the total variation, while the second component explains 25.8% (Supporting Information: Figure S3). The first principal component captures a combination of temperature and precipitation variables, with positive values corresponding to wetter and colder regions (Supporting Information: Table S6 and Figure S3). The second principal component is mainly correlated with precipitation in the coldest quarter, with positive values corresponding to drier regions during this quarter. The δ¹³C was statistically associated with the climatic first principal component, with populations inhabiting the drier and warmer habitats (negative values in the principal component analysis) having higher δ¹³C (Table 1a and Figure 2a). These results are consistent with the hypothesis that a larger proportion of carbon is fixed via the C₄ pathway in habitats favouring C₄ plants.

3.3 │ Phylogenetic lineages of non-C₄ *A. semialata* occupy different regions across the Central Zambezian miombo woodlands

Phylogenetic analyses based on data extracted from the different data sets confirmed that all non-C₄ from the Central Zambezian

region form a monophyletic group (corresponding to clade II of Olofsson et al., 2016, 2021), distinct from the non-C₄ accessions from southern Africa and C₄ individuals (Figure 3 and Supporting Information: Figure S4). Within this non-C₄ group, well-supported subclades correspond to distinct geographic regions, which mostly represent subdivisions of the two groups recognized by Olofsson et al. (2021) based on a smaller sampling (groups IIa and IIb). An accession from DRC (DRC11; new lineage IIc) is sister to all others, and a small clade containing accessions from Burundi and the middle and southern western regions of Tanzania is then sister to the rest (lineage IIb.1; Figure 3 and Supporting Information: Figure S4). The remaining accessions are separated into four, well-supported groups. The first of these contains accessions from the south of Tanzania and the north-east of Zambia (lineage IIb.2), and the second (lineage IIb.3) is located slightly west of it, expanding into DRC (Figure 3 and Supporting Information: Figure S4). The third of these groups (lineage IIa.1) includes individuals from the west of Zambia and adjacent areas from DRC, and the fourth (lineage IIa.2) is composed of Zambian accessions that are spread in the east of Zambia and neighbours the other groups (Figure 3 and Supporting Information: Figure S4). Despite their geographic separation, the six groups largely overlap in the climatic space (Supporting Information: Table S5 and Figure 3).

TABLE 1 Summary of PGLS analysis.

Response variable		PC1		PC2		R^2
(a) Summary of multiple regression analysis testing the effects of climate						
$\delta^{13}C$		−64.03 (2, 34) **<0.0001**		**NS**		0.27

Response variable	IBSF	IBSW	BSD	IBSF × Group	BSD × Group	Group	R^2
(b) Summary of multiple regression testing the effects of anatomy and phylogenetic group							
$\delta^{13}C$	3.34 (9, 99) **0.001**	4.71 (9, 99) **<0.0001**	−2.28 (9, 99) **0.02**	NS	2.57 (13, 95) **0.01**	−12.75 (9, 99) **<0.00001**	0.57

Model	IBSF		IBSW		BSD		R^2
(c) Summary of PGLS analysis testing the effects of anatomy only							
Full PGLS	1.56 (3, 26) **0.13**		3.68 (3, 26) **0.001**		−1.24 (3, 26) **0.22**		0.25
Reduced PGLS	3.80 (2, 27) **0.004**		3.13 (2, 27) **0.0007**		-		0.23

Note: For (b) and (c), the full model tested all three anatomical variables as predictors of $\delta^{13}C$, and the reduced PGLS model was rerun after removing the least significant effect (BSD). The statistics shown are t (df) p value for each variable, with bold indicating significance, and the adjusted R^2 for each model is shown.

Abbreviations: BSD, bundle sheath distance; IBSF, inner bundle sheath fraction; IBSW, inner bundle sheath width; NS, not significant; PC, principal component; PGLS, phylogenetic generalized least squares.

3.4 | Variation in leaf anatomy explains carbon isotope ratios

All sampled accessions had starch staining in the inner bundle sheaths, supporting the hypothesis based on $\delta^{13}C$ that this tissue is used for the Calvin–Benson–Bassham cycle in these individuals, although the mesophyll in some plants also stained for starch. While most non-C$_4$ individuals had only major veins (secondary and tertiary), the presence of a few minor veins was observed in some non-C$_4$ individuals (Supporting Information: Figure S5), but these never reached the large numbers observed in C$_4$ accessions of *A. semialata* (Lundgren et al., 2019). Important quantitative variation was observed among the non-C$_4$ individuals. In particular, IBSW varied from 8.3 to 17.8 µm (Supporting Information: Table S5), BSD varied from 53.5 to 230.1 µm, and the IBSF varied from 0.05 to 0.22 µm (Supporting Information: Table S5).

The variation in $\delta^{13}C$ is partially explained by anatomical variation (Figure 2 and Table 1b). Multiple regression analysis of the whole data set showed that the three variables IBSF, BSD, and IBSW together explain 57% of the variation in $\delta^{13}C$. The relationships between $\delta^{13}C$ and both IBSF and IBSW are positive, so that individuals with greater amounts of bundle sheath tissues and larger BSDs have a stronger C$_4$ pathway. Individuals with greater amounts of bundle sheath tissues and larger bundle sheath cells, therefore, have a stronger C$_4$ pathway. Conversely, the relationship between $\delta^{13}C$ and BSD is negative, so that individuals with a smaller distance between consecutive bundle sheaths have a stronger C$_4$ cycle.

In the multiple regression model, there is a significant interaction between BSD and lineage, indicating that the intercepts and slopes change among lineages (Table 1 and Figure 2b). There is an additional effect of the phylogenetic lineage for IBSF, but the interaction between IBSF and lineage is not significant, indicating that only the intercepts change among lineages (Figure 2d and Table 1). PGLS analysis using a subset of the data confirmed the multiple regression results, showing that IBSF and IBSW together explain 23% of the variation in $\delta^{13}C$, whereas the relationship with BSD is weaker and NS in the full model (Table 1c). The relationships between $\delta^{13}C$ and both IBSF and IBSW were positive and highly significant.

These results indicate that, across the studied region, individuals with anatomical traits usually associated with C$_4$ plants acquire a greater proportion of their atmospheric carbon via the C$_4$ cycle. Importantly, the same relationship is observed within a single population for which more individuals were sampled (Figure 4 and Supporting Information: Table S7). This indicates that intraspecific variation diversity provides a substrate for natural selection, and demonstrates that there is considerable variation in both $\delta^{13}C$ and anatomy at a single location experiencing the same climatic conditions.

Since $\delta^{13}C$ may also be influenced by environmental effects on water-use efficiency and bundle sheath leakiness, we explored these alternatives using a model sensitivity analysis. The analysis indicated that some of the observed variations in $\delta^{13}C$ among individuals could arise from differences in their water-use efficiency or bundle sheath leakiness (Supporting Information: Table S4).

4 | DISCUSSION

4.1 | Anatomical variation is related to the strength of the C$_4$ cycle in non-C$_4$ plants

The distribution of carbon isotopes among non-C$_4$ samples of *A. semialata* collected in the Central Zambezian miombo woodlands supports this region as an important centre of variation for
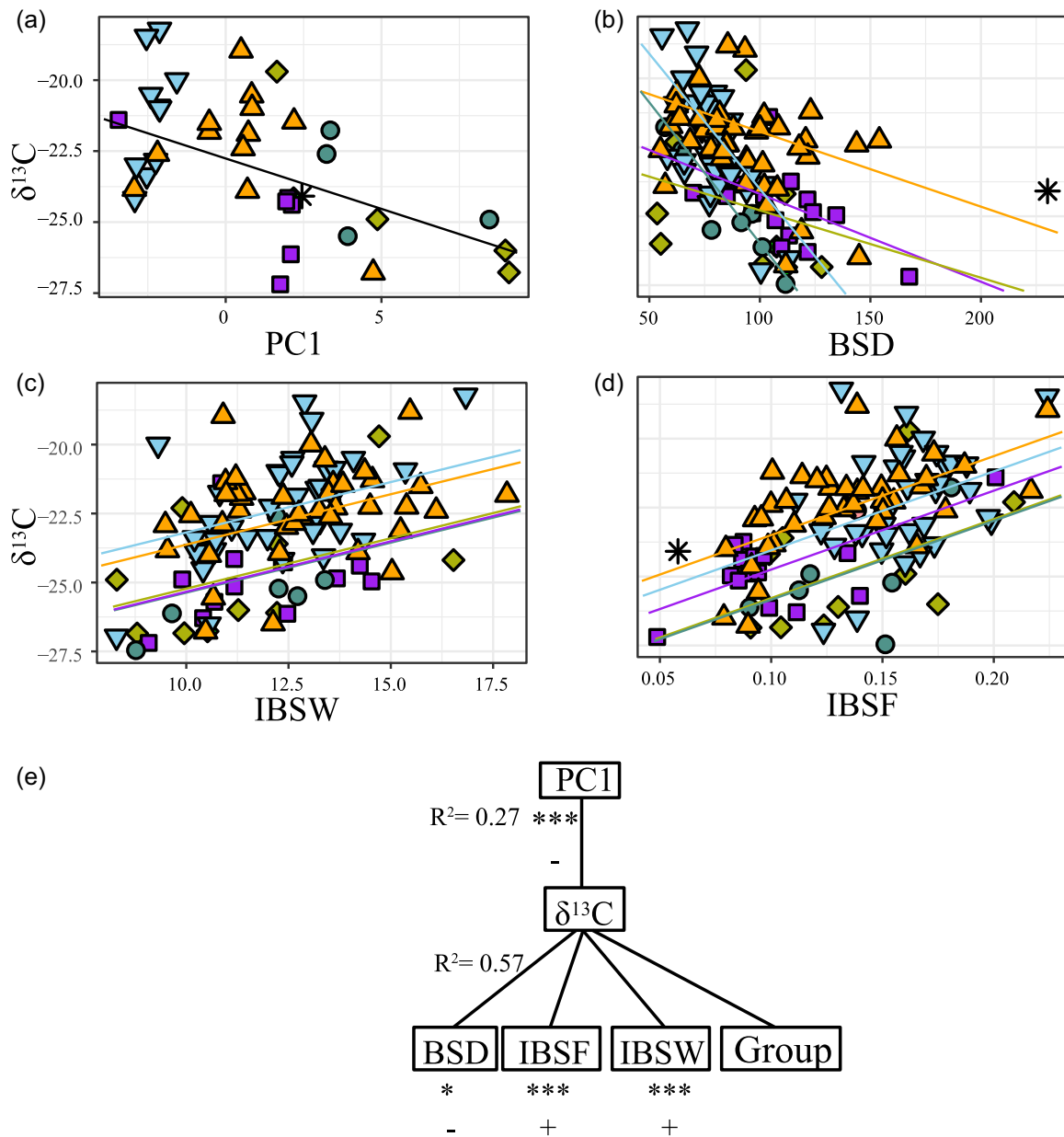
FIGURE 2 Relationships between ecology, anatomy and photosynthetic type. For the sampled non-C₄ individuals of *Alloteropsis semialata*, plots show (a) the averaged carbon isotope ratio ($\delta^{13}C$) for each population as a function of the position along the climatic first principal component (PC1), (b) the carbon isotope ratio ($\delta^{13}C$) as a function of bundle sheath distance (BSD), (c) the carbon isotope ratio ($\delta^{13}C$) as a function of inner bundle sheath width (IBSW) and (d) the carbon isotope ratio ($\delta^{13}C$) as a function of inner bundle sheath fraction (IBSF). In each case, colours and shapes indicate the main phylogenetic groups. (e) The hierarchical relationships are indicated, with in each case an indication of the directionality of the relationship (+ for positive and – for negative), its significance level (*<0.05, ***<0.001) and the model R^2. [Color figure can be viewed at wileyonlinelibrary.com]

photosynthetic types within the group (Figure 1b). The most negative values could be associated with a CO_2 fixation pathway either based on the C₃ cycle or complemented by a photorespiratory pump (also called the 'C₂ cycle'; von Caemmerer, 2000; Khoshravesh et al., 2016; Sage et al., 2012). The few individuals with low $\delta^{13}C$ values whose physiology was previously characterized had CO_2-compensation points that were not compatible with a pure C₃ type (e.g., from population TAN2; Lundgren et al., 2016, 2019). Although this does

not necessarily imply that all non-C₄ from the region have C₄ cycle activity, we can safely conclude that the C₄ cycle in these populations with a low carbon isotope ratio is at best very weak. Conversely, the numerous non-C₄ individuals with carbon isotope values greater than −23‰ unambiguously acquired a large fraction of their CO_2 via the C₄ cycle, while still using the C₃ cycle (potentially involving a photorespiratory pump) for part of their carbon acquisition (Brown & Hattersley, 1989; von Caemmerer, 1992; Farquhar et al., 1989; Stata
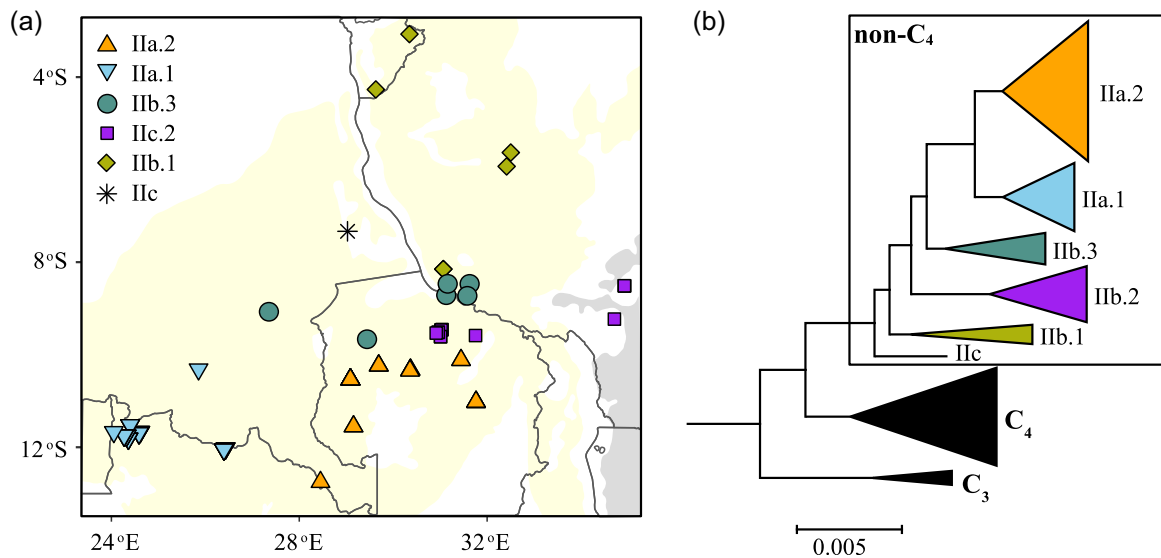
FIGURE 3 Distribution of non-C$_4$ accessions of *Alloteropsis semialata*. (a) The sampled populations are shown on a geographical map, with shapes and colours indicating the phylogenetic groups, as in Figure 2. The extent of the miombo woodlands is shown in the background, as in Figure 1. (b) Simplified phylogenetic tree, where the main non-C$_4$ lineages are collapsed and coloured as in panel a. The full phylogenetic tree is available in Supporting Information: Figure S4. [Color figure can be viewed at wileyonlinelibrary.com]
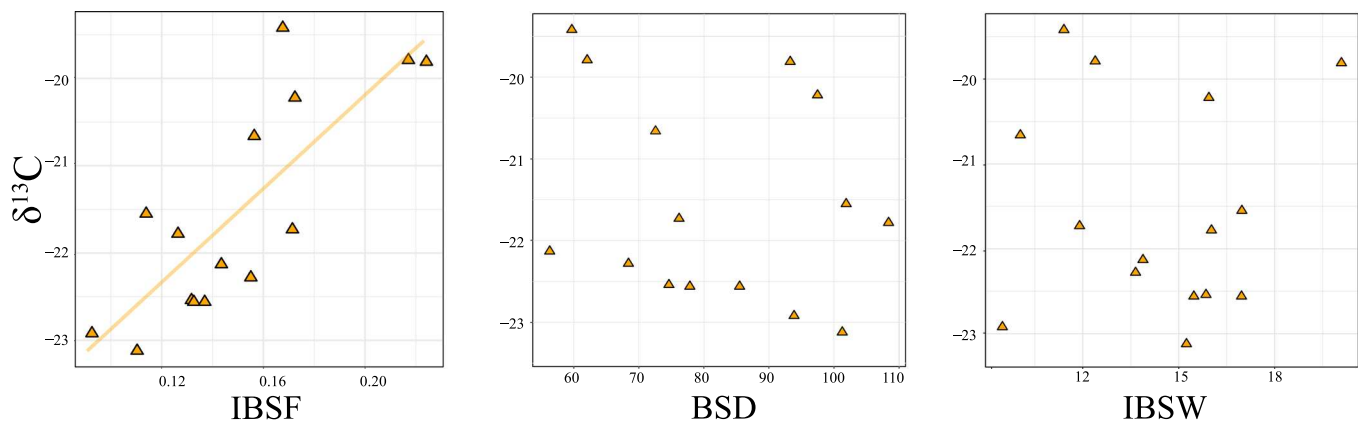

FIGURE 4 Intrapopulation variation in leaf anatomy and carbon isotope ratios. The relationship between the carbon isotope ratio ($\delta^{13}C$) and the fraction of inner bundle sheath tissue (IBSF) is shown for 15 non-C$_4$ individuals sampled within a single population (population ZAM1715). The phylogenetic generalized least-squares (PGLS) result is indicated ($p < 0.001$, $R^2 = 0.24$), but it is not significant for other anatomical traits (bundle sheath cell [BSD] and inner bundle sheath width [IBSW]). [Color figure can be viewed at wileyonlinelibrary.com]

& Sage, 2019). This intraspecific variation would provide a fertile ground for genome-wide association studies aiming to elucidate the genetic determinism of C$_4$ characters (Simpson et al., 2021), and already allows investigations about the local-scale drivers of C$_4$ activity.

Sensitivity analysis using a model of carbon isotope discrimination in C$_3$–C$_4$ intermediate plants indicated that some of the observed variation in $\delta^{13}C$ among individuals could arise from environmental effects on water-use efficiency in these field-sampled leaves. However, three lines of evidence argue against an environmental effect being the dominant cause of $\delta^{13}C$ variation. First, previous work with this species has shown that the anatomical characteristics observed here are associated with physiological values

of CO$_2$-compensation point consistent with the operation of a weak C$_4$ cycle (Lundgren et al., 2016). Second, the same study also showed that differences in $\delta^{13}C$ among genotypes in the field are preserved in a common environment, showing that they are fixed rather than plastic (Lundgren et al., 2016). Recent experiments have supported this result, by showing that the $\delta^{13}C$ values of multiple C$_3$–C$_4$ intermediate genotypes are unaffected by temperature under controlled environmental conditions (Alenazi, unpublished data). Finally, the relationships between $\delta^{13}C$ and anatomical traits are observed within a single population at a site experiencing the same climatic conditions, as well as among populations. In combination, these findings imply that, although some of the observed variations in $\delta^{13}C$ may be environmental, the primary cause is genetic differences

in leaf anatomy. However, we cannot discount the possibility that some of the differences in δ^{13}C among individuals arise from genetic variation in water-use efficiency rather than genetic variation in the strength of the C$_4$ cycle.

The characteristics of the inner bundle sheath, which is used to segregate the part of the C$_4$ cycle of *A. semialata* responsible for the release of CO$_2$ (Hattersley et al., 1977; Lundgren et al., 2019), vary among non-C$_4$ *A. semialata*, and this variation statistically explains a large part of the variation in δ^{13}C (Table 1 and Figure 2). These patterns indicate that plants with a combination of a higher fraction of the leaf dedicated to the inner bundle sheath, larger bundle sheath cells and shorter distances between consecutive bundle sheaths increase the fraction of CO$_2$ initially fixed by PEPC (which starts the C$_4$ cycle) as opposed to Rubisco (which starts the C$_3$ cycle, but also a potential photorespiratory pump). Both enzymes are present in the mesophyll cells of *A. semialata* (Lundgren et al., 2016; Ueno & Sentoku, 2006), although it is not established these are both active. The increased CO$_2$ fixation by PEPC might result from enzymatic changes, but PEPC gene expression does not vary substantially among non-C$_4$ individuals of *A. semialata* (Dunning et al., 2019). Even if small changes to enzyme expression and activity cannot be excluded, our results suggest that the strengthening of the C$_4$ biochemical cycle implied by δ^{13}C is at least partially driven by anatomical changes (Figure 2), which contradicts the widespread assumption that the transition from weak to strong C$_4$ cycle is mainly driven by the upregulation of C$_4$ enzymes (Heckmann et al., 2013; Sage, 2004). Our data suggest that quantitative changes in leaf anatomy are associated with the strength of the C$_4$ cycle in non-C$_4$ plants of *A. semialata*.

We hypothesize that leaf structural properties can shift the balance of carbon fixation towards the C$_4$ cycle. If both Rubisco and PEPC are active in the mesophyll, the enzymes will compete for CO$_2$ fixation. While the product of Rubisco can be directly processed in the mesophyll, the product of PEPC needs to be transported to the bundle sheath to be decarboxylated. Importantly, a high rate of mesophyll-to-bundle sheath transport relies on a concentration differential, with low C$_4$ acid and high C$_3$ acid concentrations in the bundle sheath cells compared to the mesophyll (Arrivault et al., 2017; Schlüter et al., 2017). A long distance between mesophyll and bundle sheath cells will hamper the diffusion of metabolites, while a small bundle sheath area will be insufficient to process the large quantities of C$_4$ acids produced in a large area of mesophyll, weakening the biochemical pull and leading to the accumulation of C$_4$ acids in the mesophyll (Bräutigam et al., 2018). These products will inhibit PEPC activity (Chollet et al., 1996), thereby favouring CO$_2$ fixation by Rubisco. Any increase of the bundle sheath area or decrease of the distance between bundle sheaths would conversely increase the strength of the C$_4$ pump, which would in turn favour CO$_2$ fixation by PEPC over Rubisco in the mesophyll (Bräutigam et al., 2016; von Caemmerer & Furbank, 1999). Our interpretation of results is that such a process increased the strength of the C$_4$ cycle in some *A. semialata* populations, providing a path from weak to strong C$_4$ activity via incremental anatomical changes (Figures 2d and 5). Importantly, our comparative analyses show that three different leaf properties are independently associated with carbon isotope ratios in *A. semialata* (Table 1 and Figure 2). This result implies that different anatomical changes are correlated with similar strengthening of the C$_4$ pathway in this species, possibly providing multiple targets for natural selection.

4.2 | Transition to stronger C$_4$ is associated with high temperatures

The higher carbon isotope ratios, which can be found in multiple phylogenetic lineages, are correlated with more negative values along
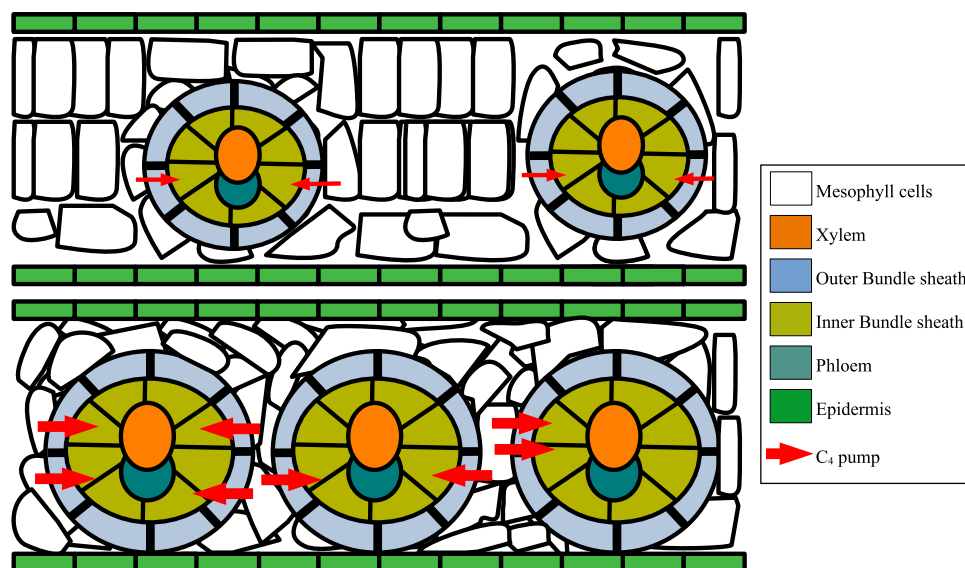

FIGURE 5 Hypothetical effect of anatomy on the strength of the C$_4$ cycle. Cross-sections are represented for two hypothetical individuals, with the bottom ones having larger bundle sheaths and shorter distances between them that increase the strength of the C$_4$ pump (represented with red arrows). [Color figure can be viewed at wileyonlinelibrary.com]

the first principal component of the analysis of climatic data (Figure 2a). These values correspond to warmer and drier environments (Figure 2a and Table 1), which are known to favour C_4 over C_3 plants (Ehleringer, 1978; Ehleringer & Björkman, 1977; Hatch, 1987; Sage, 2001; Teeri & Stowe, 1976). Previous comparative work across the whole grass family has indicated that evolutionary transitions from C_3 to C_4 photosynthesis occurred in hot environments (Edwards & Smith, 2010), have been faster in tropical than temperate climates (Watcharamongkol et al., 2018), and coincided with shifts into drier regions (Edwards & Smith, 2010). Phylogeographic analyses (Bianconi et al., 2020), grounded in previous characterizations of these populations (Lundgren et al., 2015; 2016; Olofsson et al., 2016), show that the non-C_4 group of *A. semialata* likely emerged within the Central Zambezian miombo woodlands, and has since remained tightly associated with this biome. Our new results suggest that climatic variation within this region can drive the evolution of more C_4-like types, in a process of local adaptation. Microhabitat variation linked to solar radiation and surface temperature (e.g., associated with tree cover) or heterogeneity in soil moisture (e.g., associated with soil depth or texture) might have equivalent selective effects within populations growing in the same climate. However, we do not have the fine-grained spatial data required to test this hypothesis.

The strengthening of the C_4 cycle decreases photorespiration (von Caemmerer & Furbank, 2003), which is elevated in warmer and drier areas (Ehleringer et al., 1991; Sage et al., 2012), providing the selective impetus for the observed relationships. We conclude that, as plants colonized habitats associated with increased photorespiration, anatomical changes were gradually selected to fix more CO_2 via the C_4 cycle. Over time, this led to non-C_4 populations with a strong C_4 cycle in some regions. A similar evolutionary path might have further led to plants acquiring almost all of their CO_2 via the C_4 cycle, as the C_4 group of *A. semialata* differs from the non-C_4 mainly by the presence of minor veins, which increase further the fraction of bundle sheath tissue (Lundgren et al., 2019), and the upregulation of a few genes (Dunning et al., 2019). Interestingly, the presence of sparse minor veins is detected as a rare polymorphism in some non-C_4 individuals (6.4% of the 109 individuals analysed here), which could be a result of standing genetic variation and, in a few cases, of introgression from C_4 populations (Olofsson et al., 2016). Overall, our investigations are consistent with the hypothesis that the transition from weak C_4 activity within non-C_4 individuals to fully C_4 plants can be mediated by climatic selection for anatomical changes that gradually shift the balance towards CO_2 fixation by PEPC.

Despite the overall strong relationship between anatomy and carbon isotopes, there is an additional effect of the genetic groups (Figure 2e). In particular, for a given fraction of bundle sheath, groups IIa.1e and IIa.2, and to a lesser extent IIb.2, have more positive carbon isotope ratios than the other groups (Figure 2d). While biochemical investigations are required to test this hypothesis, it is likely that this effect results from slight differences in the expression of some C_4-related enzymes. Such properties might have evolved a limited number of times and have then been mostly retained within each group. If correct, this would indicate that biochemical changes happen infrequently and therefore lead to punctuated transitions, while anatomical tuning provides a rapid path to adaptation during the evolution of C_4 photosynthesis.

5 | CONCLUSION

Our intraspecific analyses of non-C_4 *A. semialata* show that a strengthening of the C_4 cycle is statistically associated with changes in multiple leaf anatomical traits. The data are therefore consistent with the hypothesis that these changes improve the biochemical pumping of C_4 acids from mesophyll to bundle sheath cells, which shifts the fixation of CO_2 in the mesophyll towards PEPC. Importantly, stronger C_4 pathways, as detected via higher carbon isotope ratios, are correlated with warmer and drier habitats, pointing to local adaptation. Overall, these patterns suggest that, during the spread of non-C_4 *A. semialata*, habitats promoting photorespiration have selected for increased C_4 involvement. While some enzymatic changes might have happened in a punctuated manner, potentially explaining slight variation among phylogenetic lineages, our data imply that quantitative anatomical changes provided rapid evolutionary paths to physiological adaptation. Over time, such a process is likely to have led to the C_4 populations of *A. semialata* that are now found around the world.

DATA AVAILABILITY STATEMENT

The data that supports the findings of this study are available in the Supporting Information: Material of this article.

ORCID

Matheus E. Bianconi 🆔 http://orcid.org/0000-0002-1585-5947
Lara Pereira 🆔 http://orcid.org/0000-0001-5184-8587
Colin P. Osborne 🆔 http://orcid.org/0000-0002-7423-3718

REFERENCES

Arrivault, S., Obata, T., Szecówka, M., Mengin, V., Guenther, M., Hoehne, M. et al. (2017) Metabolite pools and carbon flow during C_4 photosynthesis in maize: $^{13}CO_2$ labeling kinetics and cell type fractionation. *Journal of Experimental Botany*, 68, 283–298.

Bender, M.M. (1968) Mass spectrometric studies of carbon 13 variations in corn and other grasses. *Radiocarbon*, 10, 468–472.

Bianconi, M.E., Dunning, L.T., Curran, E.V., Hidalgo, O., Powell, R.F., Mian, S. et al. (2020) Contrasted histories of organelle and nuclear genomes underlying physiological diversification in a grass species. *Proceedings of the Royal Society B: Biological Sciences*, 287, 20201960.

Bowes, G., Ogren, W.L. & Hageman, R.H. (1971) Phosphoglycolate production catalyzed by ribulose diphosphate carboxylase. *Biochemical and Biophysical Research Communications*, 45, 716–722.

Bräutigam, A., Schlüter, U., Lundgren, M.R., Flachbart, S., Ebenhöh, O. & Schönknecht, G. et al. (2018) Biochemical mechanisms driving rapid fluxes in C3–C4 photosynthesis. *BioRxiv*. [Preprint] Available from: https://doi.org/10.1101/387431 [Accessed 9th August 2018].

Brautigam, C.A., Zhao, H., Vargas, C., Keller, S. & Schuck, P. (2016) Integration and global analysis of isothermal titration calorimetry data for studying macromolecular interactions. *Nature Protocols*, 11, 882–894.

Brown, R.H. & Hattersley, P.W. (1989) Leaf anatomy of C$_3$-C$_4$ species as related to evolution of C$_4$ photosynthesis. *Plant Physiology*, 91, 1543–1550.

Brown, W.V. (1977) The Kranz syndrome and its subtypes in grass systematics. *Memoirs of the Torrey Botanical Club*, 23, 1–97.

Burnell, J.N. & Hatch, M.D. (1988) Photosynthesis in phosphoenolpyruvate carboxykinase-type C$_4$ plants: pathways of C$_4$ acid decarboxylation in bundle sheath cells of *Urochloa panicoides*. *Archives of Biochemistry and Biophysics*, 260, 187–199.

Cerling, T.E. (1999) Paleorecords of C$_4$ plants and ecosystems. In: Sage, R.F. & Monson, R.K. (Eds.) *C$_4$ plant biology*. San Diego: Academic Press, pp. 445–469.

Cerling, T.E., Harris, J.M., MacFadden, B.J., Leakey, M.G., Quade, J., Eisenmann, V. et al. (1997) Global vegetation change through the Miocene/Pliocene boundary. *Nature*, 389, 153–158.

Cerros-Tlatilpa, R. & Columbus, J.T. (2009) C$_3$ photosynthesis in *Aristida longifolia*: implication for photosynthetic diversification in Aristidoideae (Poaceae). *American Journal of Botany*, 96, 1379–1387.

Chollet, R., Vidal, J. & O'Leary, M.H. (1996) Phosphoenolpyruvate carboxylase: a ubiquitous, highly regulated enzyme in plants. *Annual Review of Plant Physiology and Plant Molecular Biology*, 47, 273–298.

Dengler, N. (1994) Quantitative leaf anatomy of C$_3$ and C$_4$ grasses (Poaceae): bundle sheath and mesophyll surface area relationships. *Annals of Botany*, 73, 241–255.

Dengler, N.G. & Nelson, T. (1999) Leaf structure and development in C$_4$ plants. In: Sage, R.F. & Monson, R.K. (Eds.) *C$_4$ plant biology*. San Diego: Academic Press, pp. 133–172.

Dunning, L.T., Lundgren, M.R., Moreno-Villena, J.J., Namaganda, M., Edwards, E.J., Nosil, P. et al. (2017) Introgression and repeated co-option facilitated the recurrent emergence of C$_4$ photosynthesis among close relatives. *Evolution*, 71, 1541–1555.

Dunning, L.T., Moreno-Villena, J.J., Lundgren, M.R., Dionora, J., Salazar, P., Adams, C. et al. (2019) Key changes in gene expression identified for different stages of C$_4$ evolution in *Alloteropsis semialata*. *Journal of Experimental Botany*, 70, 3255–3268.

Edwards, E.J. & Smith, S.A. (2010) Phylogenetic analyses reveal the shady history of C$_4$ grasses. *Proceedings of the National Academy of Sciences*, 107, 2532–2537.

Edwards, G.E. & Ku, M.S. (1987) Biochemistry of C$_3$–C$_4$ intermediates. In: Hatch, M.D. & Boardman (Eds.) *The biochemistry of plants: a comprehensive treatise*, vol. 10. New York: Academic Press, pp. 275–325.

Ehleringer, J. & Björkman, O. (1977) Quantum yields for CO$_2$ uptake in C$_3$ and C$_4$ plants: dependence on temperature, CO$_2$, and O$_2$ concentration. *Plant Physiology*, 59, 86–90.

Ehleringer, J.R. (1978) Implications of quantum yield differences on the distributions of C$_3$ and C$_4$ grasses. *Oecologia*, 31, 255–267.

Ehleringer, J.R., Sage, R.F., Flanagan, L.B. & Pearcy, R.W. (1991) Climate change and the evolution of C$_4$ photosynthesis. *Trends in Ecology & Evolution*, 6, 95–99.

Ellis, R.P. (1974) Anomalous vascular bundle sheath structure in *Alloteropsis semialata* leaf blades. *Bothalia*, 11, 273–275.

Farquhar, G.D., Ehleringer, J.R. & Hubick, K.T. (1989) Carbon isotope discrimination and photosynthesis. *Annual Review of Plant Physiology and Plant Molecular Biology*, 40, 503–537.

Farquhar, G.D., O'Leary, M.H. & Berry, J.A. (1982) On the relationship between carbon isotope discrimination and the intercellular carbon dioxide concentration in leaves. *Australian Journal of Plant Physiology*, 9, 121–137.

Fick, S.E. & Hijmans, R.J. (2017) WorldClim 2: new 1-km spatial resolution climate surfaces for global land areas. *International Journal of Climatology*, 37, 4302–4315.

Gowik, U., Bräutigam, A., Weber, K.L., Weber, A.P.M. & Westhoff, P. (2011) Evolution of C$_4$ photosynthesis in the genus *Flaveria*: how many and which genes does it take to make C$_4$? *The Plant Cell*, 23, 2087–2105.

Gutiérrez-Rodríguez, A., Latasa, M., Mourre, B. & Laws, E. (2009) Coupling between phytoplankton growth and microzooplankton grazing in dilution experiments: potential artefacts. *Marine Ecology Progress Series*, 383, 1–9.

Guy, R.D., Reid, D.M. & Krouse, H.R. (1980) Shifts in carbon isotope ratios of two C$_3$ halophytes under natural and artificial conditions. *Oecologia*, 44(2), 241–247. http://www.jstor.org/stable/4216017

Hatch, M. & Slack, C. (1966) Photosynthesis by sugar-cane leaves. A new carboxylation reaction and the pathway of sugar formation. *Biochemical Journal*, 101, 103–111.

Hatch, M.D. (1971) The C$_4$ pathway of photosynthesis. Evidence for an intermediate pool of carbon dioxide and the identity of the donor C$_4$ dicarboxylic acid. *Biochemical Journal*, 125, 425–432.

Hatch, M.D. (1987) C$_4$ photosynthesis: a unique blend of modified biochemistry, anatomy and ultrastructure. *Biochimica et Biophysica Acta/Bioenergetics*, 895, 81–106.

Hatch, M.D. & Osmond, C.B. (1976) Compartmentation and transport in C$_4$ photosynthesis. In: Stocking, C.R. & Heber, U. (Eds.) *Transport in plants III: intracellular interactions and transport processes*, vol. 144. Berlin, Heidelberg: Springer, p. 184.

Hattersley, P.W. (1984) Characterization of C$_4$ type leaf anatomy in grasses (Poaceae). Mesophyll: bundle sheath area ratios. *Annals of Botany*, 53, 163–180.

Hattersley, P.W. & Watson, L. (1975) Anatomical parameters for predicting photosynthetic pathways of grass leaves: the "maximum lateral cell count" and the "maximum cells distant count". *Phytomorphology*, 25, 325–333.

Hattersley, P.W., Watson, L. & Osmond, C.B. (1977) In situ immunofluorescent labelling of Ribulose-1,5-bisphosphate carboxylase in leaves of C$_3$ and C$_4$ plants. *Australian Journal of Plant Physiology*, 4, 523–539.

Heckmann, D., Schulze, S., Denton, A., Gowik, U., Westhoff, P., Weber, A.P.M. et al. (2013) Predicting C$_4$ photosynthesis evolution: modular, individually adaptive steps on a Mount Fuji fitness landscape. *Cell*, 153, 1579–1588.

Hijmans, R.J. (2021) *Geographic data analysis and modeling R package raster version 3.4-10*. Accessed March 16, 2023. https://cran.r-project.org/web/packages/raster/index.html

Hugin Development Team. (2015) *Hugin - Panorama photo stitcher*. https://hugin.sourceforge.io

Kennedy, R.A. & Laetsch, W.M. (1974) Plant species intermediate for C$_3$, C$_4$ photosynthesis. *Science*, 184, 1087–1089.

Khoshravesh, R., Stinson, C.R., Stata, M., Busch, F.A., Sage, R.F., Ludwig, M. et al. (2016) C$_3$–C$_4$ intermediacy in grasses: organelle enrichment and distribution, glycine decarboxylase expression, and the rise of C$_2$ photosynthesis. *Journal of Experimental Botany*, 67, 3065–3078.

Ku, M.S.B., Monson, R.K., Littlejohn Jr., R.O., Nakamoto, H., Fisher, D.B. & Edwards, G.E. (1983) Photosynthetic characteristics of C$_3$–C$_4$ intermediate *Flaveria* species: I. Leaf anatomy, photosynthetic

responses to O_2 and CO_2, and activities of key enzymes in the C_3 and C_4 pathways. *Plant Physiology*, 71, 944–948.

Langmead, B. & Salzberg, S.L. (2012) Fast gapped-read alignment with Bowtie 2. *Nature Methods*, 9, 357–359.

Li, H., Handsaker, B., Wysoker, A., Fennell, T., Ruan, J., Homer, N. et al. (2009) The sequence alignment/Map format and SAMtools. *Bioinformatics*, 25, 2078–2079.

Lorimer, G.H. & Andrews, T.J. (1973) Plant photorespiration—an inevitable consequence of the existence of atmospheric oxygen. *Nature*, 243, 359–360.

Lundgren, M.R., Besnard, G., Ripley, B.S., Lehmann, C.E.R., Chatelet, D.S., Kynast, R.G. et al. (2015) Photosynthetic innovation broadens the niche within a single species. *Ecology Letters*, 18, 1021–1029.

Lundgren, M.R., Christin, P.A., Escobar, E.G., Ripley, B.S., Besnard, G., Long, C.M. et al. (2016) Evolutionary implications of C_3–C_4 intermediates in the grass *Alloteropsis semialata*. *Plant, Cell & Environment*, 39, 1874–1885.

Lundgren, M.R., Dunning, L.T., Olofsson, J.K., Moreno-Villena, J.J., Bouvier, J.W., Sage, T.L. et al. (2019) C_4 anatomy can evolve via a single developmental change. *Ecology Letters*, 22, 302–312.

Lundgren, M.R., Osborne, C.P. & Christin, P.-A. (2014) Deconstructing Kranz anatomy to understand C_4 evolution. *Journal of Experimental Botany*, 65, 3357–3369.

Maquia, I., Catarino, S., Pena, A.R., Brito, D.R.A., Ribeiro, N.S., Romeiras, M.M. et al. (2019) Diversification of African tree legumes in Miombo–Mopane Woodlands. *Plants*, 8, 182.

Monson, R.K. & Edwards, G.E. (1984) C_3–C_4 intermediate photosynthesis in plants. *BioScience*, 34, 563–574.

Monson, R.K. & Moore, B. (1989) On the significance of C_3–C_4 intermediate photosynthesis to the evolution of C_4 photosynthesis. *Plant, Cell & Environment*, 12, 689–699.

Monson, R.K., Moore, B., KU, M.S.B. & Edwards, G.E. (1986) Co-function of C_3 and C_4 photosynthetic pathways in C_3, C_4 and C_3-C_4 intermediate *Flaveria* species. *Planta*, 168, 493–502.

Monson, R.K., Teeri, J.A., Ku, M.S.B., Gurevitch, J., Mets, L.J. & Dudley, S. (1988) Carbon-isotope discrimination by leaves of *Flaveria* species exhibiting different amounts of C_3- and C_4-cycle co-function. *Planta*, 174, 145–151.

O'Leary, M.H. (1981) Carbon isotope fractionation in plants. *Phytochemistry*, 20(4), 553–567.

Olofsson, J.K., Bianconi, M., Besnard, G., Dunning, L.T., Lundgren, M.R., Holota, H. et al. (2016) Genome biogeography reveals the intraspecific spread of adaptive mutations for a complex trait. *Molecular Ecology*, 25, 6107–6123.

Olofsson, J.K., Cantera, I., de Paer, C., Hong-Wa, C., Zedane, L. & Dunning, L.T. et al. (2019) Phylogenomics using low-depth whole genome sequencing: a case study with the olive tribe. *Molecular Ecology Resources*, 19, 877–892.

Olofsson, J.K., Curran, E.V., Nyirenda, F., Bianconi, M.E., Dunning, L.T., Milenkovic, V. et al. (2021) Low dispersal and ploidy differences in a grass maintain photosynthetic diversity despite gene flow and habitat overlap. *Molecular Ecology*, 30, 2116–2130.

Olofsson, J.K., Dunning, L.T., Lundgren, M.R., Barton, H.J., Thompson, J. & Cuff, N. et al. (2019) Population-specific selection on standing variation generated by lateral gene transfers in a grass. *Current Biology*, 29, 3921–3927.

Orme, D., Freckleton, R., Thomas, G., Petzoldt, T., Fritz, S. & Isaac, N. et al. (2022) *Comparative analyses of phylogenetics and evolution in R.* Available at: https://cran.r-project.org/web/packages/caper/vignettes/caper.pdf [Accessed 13th February 2023].

Peixoto, M.M., Sage, T.L., Busch, F.A., Pacheco, H.D.N., Moraes, M.G., Portes, T.A. et al. (2021) Elevated efficiency of C_3 photosynthesis in bamboo grasses: a possible consequence of enhanced refixation of photorespired CO_2. *GCB Bioenergy*, 13, 941–954.

R Core Team. (2018) *R: a language and environment for statistical computing*. Vienna, Austria: R foundation for statistical computing. Available from: https://www.R-project.org/

R Core Team. (2020) *The R Project for Statistical Computing*. https://www.r-project.org

Sage, R.F. (2001) Environmental and evolutionary preconditions for the origin and diversification of the C_4 photosynthetic syndrome. *Plant Biology*, 3, 202–213.

Sage, R.F. (2004) The evolution of C_4 photosynthesis. *New Phytologist*, 161, 341–370.

Sage, R.F., Christin, P.-A. & Edwards, E.J. (2011) The C4 plant lineages of planet Earth. *Journal of Experimental Botany*, 62, 3155–3169.

Sage, R.F., Khoshravesh, R. & Sage, T.L. (2014) From proto-Kranz to C_4 Kranz: building the bridge to C_4 photosynthesis. *Journal of Experimental Botany*, 65, 3341–3356.

Sage, R.F., Sage, T.L & Kocacinar, F. (2012) Photorespiration and the evolution of C_4 photosynthesis. *Annual Review of Plant Biology*, 63, 19–47.

Sayre, R.T. & Kennedy, R.A. (1977) Ecotypic differences in the C_3 and C_4 photosynthetic activity in *Mollugo verticillata*, a C_3–C_4 intermediate. *Planta*, 134, 257–262.

Schlüter, U., Bräutigam, A., Gowik, U., Melzer, M., Christin, P.-A., Kurz, S. et al. (2017) Photosynthesis in C_3-C_4 intermediate *Moricandia* species. *Journal of Experimental Botany*, 68, 191–206.

Schneider, C.A., Rasband, W.S. & Eliceiri, K.W. (2012) NIH Image to ImageJ: 25 years of image analysis. *Nature Methods*, 9, 671–675.

Simpson, C.J.C., Reeves, G., Tripathi, A., Singh, P. & Hibberd, J.M. (2021) Using breeding and quantitative genetics to understand the C_4 pathway. *Journal of Experimental Botany*, 73, 3072–3084.

Smith, B.N. & Brown, W.V. (1973) The Kranz syndrome in the Gramineae as indicated by carbon isotopic ratios. *American Journal of Botany*, 60, 505–513.

Smith, B.N. & Epstein, S. (1971) Two categories of $^{13}C/^{12}C$ ratios for higher plants. *Plant Physiology*, 47, 380–384.

Stamatakis, A. (2014) RAxML version 8: a tool for phylogenetic analysis and post-analysis of large phylogenies. *Bioinformatics*, 30, 1312–1313.

Stata, M., Sage, T.L. & Sage, R.F. (2019) Mind the gap: the evolutionary engagement of the C_4 metabolic cycle in support of net carbon assimilation. *Current Opinion in Plant Biology*, 49, 27–34.

Teeri, J.A. & Stowe, L.G. (1976) Climatic patterns and the distribution of C_4 grasses in North America. *Oecologia*, 23, 1–12.

Troughton, J.H. (1979) $\delta^{13}C$ as an indicator of carboxylation reactions. In: Gibbs, M. & Latzko, E. (Eds.) *Photosynthesis II. Encyclopedia of plant physiology*. Berlin: Springer.

Ueno, O. & Sentoku, N. (2006) Comparison of leaf structure and photosynthetic characteristics of C_3 and C_4 *Alloteropsis semialata* subspecies. *Plant, Cell & Environment*, 29, 257–268.

von Caemmerer, S. (1992) Carbon isotope discrimination in C_3–C_4 intermediates. *Plant, Cell & Environment*, 15, 1063–1072.

von Caemmerer, S. (2000) *Biochemical models of leaf photosynthesis*. Collingwood: CSIRO.

von Caemmerer, S. & Furbank, R.T. (1999) The modelling of C_4 photosynthesis. In: Sage, R.F. & Monson, R.K. (Eds.) C_4 *plant biology*. San Diego: Academic Press, pp. 173–211.

von Caemmerer, S. & Furbank, R.T. (2003) The C_4 pathway: an efficient CO_2 pump. *Photosynthesis Research*, 77, 191–207.

Watcharamongkol, T., Christin, P.-A. & Osborne, C.P. (2018) C_4 photosynthesis evolved in warm climates but promoted migration to cooler ones. *Ecology Letters*, 21, 376–383.

Williams, B.P., Johnston, I.G., Covshoff, S. & Hibberd, J.M. (2013) Phenotypic landscape inference reveals multiple evolutionary paths to C_4 photosynthesis. *eLife*, 2, e00961.

Winter, K. (1981) CO_2 and Water Vapour Exchange, Malate Content and δ13C Value in Cicer arietinum: Grown under Two Water Regimes. *Zeitschrift für Pflanzenphysiologie*, 101(5), 421–430.

Plant, Cell & Environment PC&E –WILEY $\mid$

Yorimitsu, Y., Kadosono, A., Hatakeyama, Y., Yabiku, T. & Ueno, O. (2019) Transition from C$_3$ to proto-Kranz to C$_3$–C$_4$ intermediate type in the genus *Chenopodium* Chenopodiaceae. *Journal of Plant Research*, 132, 839–855.

SUPPORTING INFORMATION

Additional supporting information can be found online in the Supporting Information section at the end of this article.